Accurate Excitation Energies of Point Defects from Fast Particle-Particle Random Phase Approximation Calculations

Jiachen Li,[*,†] Yu Jin,[‡] Jincheng Yu,[¶] Weitao Yang,[*,¶] and Tianyu Zhu[*,†]

†*Department of Chemistry, Yale University, New Haven, CT, USA 06520*

‡*Department of Chemistry, University of Chicago, Chicago, Illinois 60637, United States*

¶*Department of Chemistry, Duke University, Durham, NC 27708, USA*

E-mail: jiachen.li@yale.edu; weitao.yang@duke.edu; tianyu.zhu@yale.edu

Abstract

We present an efficient particle-particle random phase approximation (ppRPA) approach that predicts accurate excitation energies of point defects, including the nitrogen-vacancy (NV^-) and the silicon-vacancy (SiV^0) centers in diamond and the divacancy center (VV^0) in 4H silicon carbide, with errors within 0.2 eV compared with experimental values. Starting from the $(N+2)$-electron ground state calculated with the density functional theory (DFT), the ppRPA excitation energies of the N-electron system are calculated as the differences between the two-electron removal energies of the $(N+2)$-electron system. We demonstrate that the ppRPA excitation energies converge rapidly with a few hundred of canonical active-space orbitals. We also show that active-space ppRPA has weak DFT starting-point dependence and is significantly cheaper than the corresponding ground-state DFT calculation. This work establishes ppRPA as an accurate and low-cost tool for investigating excited-state properties of point defects and opens up new opportunities for applications of ppRPA to periodic bulk materials.

TOC Graphic

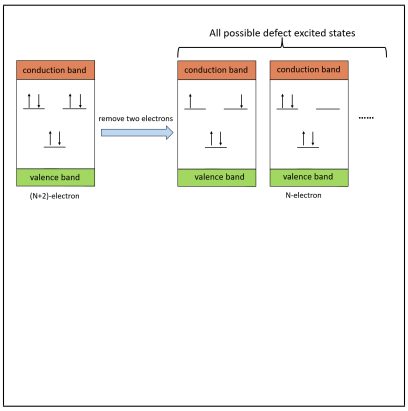

Optically addressable point defects in semiconductors and insulators have gained increasing attention due to their unique optical and magnetic properties and promises for realizing quantum technologies.[1–3] In many point defect systems, the energy levels of the defect are within the fundamental band gap of the host material, which leads to long spin coherence time even at room temperature. The spin states of point defects can also be initialized, manipulated, and read out through optical excitations. As a result, point defects have the potential to function as quantum bits (qubits) for quantum computation and single-photon emitters for quantum communication.[4–7] However, predicting optical properties of point defects from first principles remains challenging.[8] Due to the fact that defect excited states often have multiconfigurational character, a balanced treatment of static and dynamical electron correlation is required for accurately describing these states. Moreover, large supercells with hundreds of atoms are typically required to avoid interactions between periodic images and simulate in the dilute limit, which is not feasible for correlated quantum chemistry methods.

Due to high computational efficiency, excited-state extensions of the density functional theory (DFT),[9–11] including spin-conserving and spin-flip time-dependent DFT (TDDFT) as well as ΔSCF, have been widely used to describe optical properties of point defects such as vertical excitation energies, zero-phonon lines, optical spectra, and excited-state geometries.[12–17] However, it is challenging for the single-determinant-based DFT formalism to describe the strongly correlated defect states with multiconfigurational character. Moreover, TDDFT has an undesired significant starting-point dependence on the exchange-correlation functional. Periodic many-body treatments of defect excited states have been explored using the Bethe-Salpeter equation (BSE) combined with GW,[18,19] the equation-of-motion coupled-cluster theory,[20] as well as the quantum Monte Carlo approach.[21] However, the high computational costs have limited further applications of these methods. To describe the correlated defect systems with affordable cost, many flavors of quantum embedding approaches have been developed. In quantum embedding theories, a chosen active space representing the

manifold of defect states is treated by accurate but computationally demanding high-level theories, while the rest of the system is treated by cheaper low-level theories.[22–25] It has been shown that the quantum defect embedding theory (QDET),[26–28] the density matrix embedding theory (DMET),[29–31] the constrained random phase approximation (CRPA) combined with exact diagonalization (ED)[32,33] and the regional embedding theory[34] have achieved mixed successes for simulating point defect systems. Recently, a dynamical downfolding approach has been developed to treat localized correlated electronic states in the otherwise weakly correlated host medium.[35]

The particle-particle random phase approximation (ppRPA) formalism, originally developed for describing nuclear many-body interactions,[36,37] has been successfully applied to describe ground-state electron correlation as well as excited-state energies and oscillator strengths in quantum chemistry.[38–40] ppRPA can be derived from different approaches, including the equation of motion,[36,41] the adiabatic connection[38,39] and TDDFT with the pairing field.[42] As the counterpart of the commonly used particle-hole random phase approximation (phRPA),[43,44] ppRPA describes the response of the pairing matrix to a perturbation in the form of a pairing field, which conveys information in the particle-particle and the hole-hole channel. For ground states, the ppRPA correlation energy is shown to be equivalent to the ladder-coupled-cluster doubles.[45,46] In addition, ppRPA is the first known functional that captures the energy derivative discontinuity in strongly correlated systems.[38] For excited-state properties, the two-electron addition energy and the two-electron removal energy are obtained by solving the ppRPA working equation instead of the excitation energy in the particle-hole channel. Therefore, the excitation energy of the N-electron system can be obtained in two different manners: a) the particle-particle channel with the difference between two-electron addition energies of the $(N-2)$-electron system,[40] and b) the hole-hole channel with the difference between two-electron addition energies of the $(N+2)$-electron system,[40,47,48] where N is the number of electrons. It has been shown that ppRPA predicts accurate excited-state properties of molecular systems, including valence, double, Rydberg

and charge transfer excitation energies,[40,49–54] analytic gradients,[55] conical intersections,[40] oscillator strengths,[56] and spin-state energetics.[57] Recently, ppRPA with the Tamm-Dancoff approximation (TDA) has been applied in the multi-reference DFT approach to describe dissociation breakings and to predict excitation energies.[58,59] ppRPA is also used in the Green's function formalism, where the self-energy in the T-matrix approximation is formulated with the ppRPA eigenvalues and eigenvectors to calculate quasiparticle energies.[54,60–63]

The computational cost of the ppRPA approach can also be significantly reduced using the active-space formalism.[53,54] In the recently developed active-space formalism, only the particle and hole pairs with large contributions to low-lying excitation energies are included by constraining both indices in particle and hole pairs. It has been shown that using an active space of only 30 occupied and 30 virtual orbitals, active-space ppRPA achieves fast convergence to within 0.05 eV compared to full ppRPA for molecular excitations of different characters, including charge-transfer, Rydberg, double, and valence excitations as well as diradicals.[54] As a result, the ppRPA calculations for molecular excitations becomes linear scaling and is more efficient than the ground state SCF calculations of the same molecules.

In this work, we apply the active-space ppRPA approach to predict vertical excitation energies in solid-state point defects, including the negatively charged nitrogen-vacancy center (NV^-) and the neutral silicon-vacancy center (SiV^0) in diamond, and the kk-configuration of the neutral divacancy center (kk-VV^0) in 4H silicon carbide (4H-SiC). Here, the $(N+2)$-electron ground state is computed with DFT and is used as the reference in ppRPA calculations. By adding two electrons to the original N-electron defect system, the ground state becomes closed-shell, which can be straightforwardly described by single-determinant Kohn-Sham DFT. All desired excitation energies can then be obtained by taking the differences between two-electron removal energies of the $(N+2)$-electron system. We demonstrate that the excitation energy converges rapidly with respect to the size of the active space using supercells of various sizes. With a small active space consisting of only 200 occupied and 200 virtual orbitals, ppRPA predicts accurate excitation energies for all tested defect systems.

To the best of our knowledge, this work is the first application of ppRPA for excitation energies in realistic periodic bulk systems.

We first review the ppRPA formalism. As the counterpart of phRPA formulated in the particle-hole channel, ppRPA is formulated with the particle-particle propagator that completely describes the dynamic fluctuation of the pairing matrix.[38,39] In the frequency space, the time-ordered pairing matrix fluctuation is[38,39]

$$K_{pqrs}(\omega) = \sum_m \frac{\langle \Psi_0^N | \hat{a}_p \hat{a}_q | \Psi_0^{N+2} \rangle \langle \Psi_0^{N+2} | \hat{a}_s^\dagger \hat{a}_r^\dagger | \Psi_0^N \rangle}{\omega - \Omega_m^{N+2} + i\eta} - \sum_m \frac{\langle \Psi_0^N | \hat{a}_s^\dagger \hat{a}_r^\dagger | \Psi_0^{N-2} \rangle \langle \Psi_0^{N-2} | \hat{a}_p \hat{a}_q | \Psi_0^N \rangle}{\omega - \Omega_m^{N-2} - i\eta} \tag{1}$$

where $\hat{a}_p^\dagger$ and $\hat{a}_p$ are the second quantization creation and annihilation operators, $\Omega^{N\pm2}$ is the two-electron addition/removal energy, and η is a positive infinitesimal number. In Eq. 1 and the following, we use i, j, k, l for occupied orbitals, a, b, c, d for virtual orbitals, p, q, r, s for general molecular orbitals, and m for the index of the two-electron addition/removal energy.

Similar to the phRPA, the pairing matrix fluctuation K of the interacting system can be approximated from the non-interacting K_0 with the Dyson equation[38,39]

$$K = K^0 + K^0 V K \tag{2}$$

where the antisymmetrized interaction $V_{pqrs} = \langle pq||rs\rangle = \langle pq|rs\rangle - \langle pq|sr\rangle$ is used and $\langle pq|rs\rangle = \int dx_1 dx_2 \frac{\phi_p^*(x_1)\phi_q^*(x_2)\phi_r(x_1)\phi_s(x_2)}{|r_1 - r_2|}$. The direct ppRPA can be obtained by neglecting the exchange term in V in Eq. 2.[64]

Eq. 2 can be cast into a generalized eigenvalue equation, which is similar to the Casida equation in TDDFT[65,66]

$$\begin{bmatrix} \mathbf{A} & \mathbf{B} \\ \mathbf{B}^{\mathrm{T}} & \mathbf{C} \end{bmatrix} \begin{bmatrix} \mathbf{X} \\ \mathbf{Y} \end{bmatrix} = \Omega^{N\pm2} \begin{bmatrix} \mathbf{I} & \mathbf{0} \\ \mathbf{0} & -\mathbf{I} \end{bmatrix} \begin{bmatrix} \mathbf{X} \\ \mathbf{Y} \end{bmatrix} \tag{3}$$

with

$$A_{ab,cd} = \delta_{ac}\delta_{bd}(\epsilon_a + \epsilon_b) + \langle ab||cd\rangle \tag{4}$$

$$B_{ab,kl} = \langle ab||kl\rangle \tag{5}$$

$$C_{ij,kl} = -\delta_{ik}\delta_{jl}(\epsilon_i + \epsilon_j) + \langle ij||kl\rangle \tag{6}$$

where $a < b$, $c < d$, $i < j$, $k < l$ and $\Omega^{N\pm2}$ is the two-electron addition/removal energy. In our ppRPA calculations of defect systems, the DFT self-consistent field (SCF) calculation of the $(N + 2)$-electron state at the ground-state geometry of N-electron system is first performed, then the orbital energies and orbitals are used in the working equation Eq. 3 for calculating two-electron removal energies. The excitation energy can be obtained from the difference between the lowest and a higher two-electron removal energy.

Since the corresponding $(N + 2)$-electron system is closed-shell, Eq. 3 can be expressed in the spin-adapted form.[49] The singlet ppRPA matrix is given by

$$A^{\mathrm{s}}_{ab,cd} = \delta_{ac}\delta_{bd}(\epsilon_a + \epsilon_b) + \langle ab||cd\rangle \tag{7}$$

$$B^{\mathrm{s}}_{ab,kl} = \langle ab||kl\rangle \tag{8}$$

$$C^{\mathrm{s}}_{ij,kl} = -\delta_{ik}\delta_{jl}(\epsilon_i + \epsilon_j) + \langle ij||kl\rangle \tag{9}$$

with $a < b$, $c < d$, $i < j$ and $k < l$. And the triplet ppRPA matrix is given by

$$A^{\mathrm{t}}_{ab,cd} = \delta_{ac}\delta_{bd}(\epsilon_a + \epsilon_b) + \frac{1}{\sqrt{(1+\delta_{ab})(1+\delta_{cd})}}(\langle ab|cd\rangle + \langle ab|dc\rangle) \tag{10}$$

$$B^{\mathrm{t}}_{ab,kl} = \frac{1}{\sqrt{(1+\delta_{ab})(1+\delta_{kl})}}(\langle ab|kl\rangle + \langle ab|lk\rangle) \tag{11}$$

$$C^{\mathrm{t}}_{ij,kl} = -\delta_{ik}\delta_{jl}(\epsilon_i + \epsilon_j) + \frac{1}{\sqrt{(1+\delta_{ij})(1+\delta_{kl})}}(\langle ij|kl\rangle + \langle ij|lk\rangle) \tag{12}$$

with $a \leq b$, $c \leq d$, $i \leq j$ and $k \leq l$.

As introduced in Ref. 54, the ppRPA matrix can be constructed in an active space that

constrains indices of both particle and hole pairs. This means that for singlet ppRPA matrix in Eq. 7 to Eq. 9, the indices are constrained as

$$a < b \leq N_{\text{vir,act}} \text{ and } c < d \leq N_{\text{vir,act}} \tag{13}$$

$$i < j \leq N_{\text{occ,act}} \text{ and } k < l \leq N_{\text{occ,act}} \tag{14}$$

where $N_{\text{occ,act}}$ and $N_{\text{vir,act}}$ are the numbers of occupied and virtual orbitals in the active space. For the triplet ppRPA matrix in Eq. 10 to Eq. 12, the indices are constrained in the same way. As shown in Ref. 54, the above active space only includes the particle and hole pairs with large contributions to low-lying excitation energies, which greatly reduces the computational cost of the ppRPA calculations. The scaling of active-space ppRPA is $\mathcal{O}(N_{\text{act}}^4)$ using the Davidson algorithm[50,67] with N_{act} being a small number of active-space orbitals. In this work, the full diagonalization was used for ppRPA calculations due to the small size of the active space. For systems that require a larger active space, Eq. 3 can be solved with the Davidson algorithm[50] to reduce the computational cost. In addition, the AO-to-MO transformation step scales as $\mathcal{O}(N_{\text{aux}}N_{\text{AO}}^2N_{\text{act}})$ with density fitting, where N_{AO} and N_{aux} are the numbers of computational and auxiliary basis functions.

Ground-state geometries of all three defect systems were optimized with the PBE functional[68] using the Quantum ESPRESSO package,[69,70] and details can be found in the Supporting Information (SI). We then performed all $(N+2)$-electron ground-state DFT calculations in periodic Gaussian basis sets with Gaussian density fitting using the PySCF quantum chemistry software package,[71,72] in supercell calculations with Γ-point sampling. Two functionals (PBE[68] and B3LYP[73,74]) were used, in combination with the cc-pVDZ basis set[75] and the cc-pVDZ-RI auxiliary basis set.[76] As shown in Section. 3 in the SI, using cc-pVTZ basis set leads to very close results as using the cc-pVDZ basis set. With the electron integrals and DFT results obtained from PySCF, we further performed active-space ppRPA calculations with periodic boundary conditions to predict vertical excitation energies of point defects

using the Lib_ppRPA library.[77] Data from ppRPA basis set convergence tests can be found in the SI.

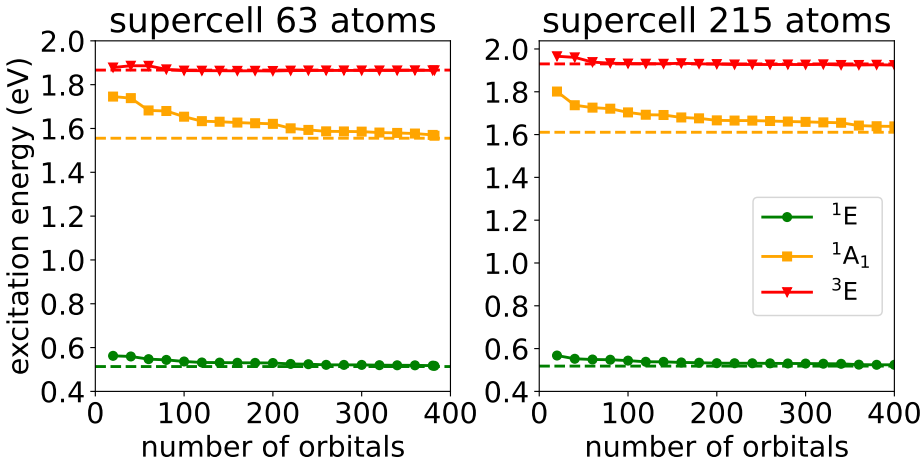

Figure 1: Vertical excitation energies of NV^- in diamond obtained from ppRPA@PBE with respect to the number of orbitals in the active space. The numbers of occupied and virtual orbitals in the active space are the same. Left: supercell containing 63 atoms. Full $(N+2)$-electron state has 191 occupied and 693 virtual orbitals. In the last point, 191 occupied and 200 virtual orbitals are included in the active space. The dashed lines correspond to excitation energies obtained from the active space with 191 occupied and 300 virtual orbitals. Right: supercell containing 215 atoms. Full $(N+2)$-electron state has 647 occupied and 2363 virtual orbitals. The dashed lines correspond to excitation energies obtained from the active space with 300 occupied and 300 virtual orbitals.

We first examine the convergence behavior of the excitation energies obtained from the ppRPA approach with respect to the size of the active space. The active-space ppRPA@PBE excitation energies of NV^- center using supercells containing 63 and 215 atoms are shown in Fig. 1. The supercell containing 63 atoms has 191 occupied and 691 virtual orbitals, while the 215-atom supercell has 647 occupied and 2363 virtual orbitals. For simplicity, the active spaces used in this work include the same numbers of occupied and virtual orbitals. As seen in Fig. 1, the excitation energies of all three excited states (i.e., ^{1}E, ^{1}A$_1$, and ^{3}E) converge rapidly with respect to the size of the active space for both supercell sizes. For the low-lying singlet excited state ^{1}E and triplet excited state ^{3}E, using an active space consisting of only 30 occupied and 30 virtual orbitals gives errors of only 0.03 eV compared with much larger active-space results (i.e., 191 occupied and 300 virtual orbitals), which is

the same as the convergence behavior for excitation energies in molecular systems reported in Ref. 54. For the $^1A_1$ excited state, slightly slower convergence is observed. Nevertheless, the ppRPA@PBE $^1A_1$ excitation energy is converged to within 0.03 eV when using 200 (191 for 63-atom supercell) occupied and 200 virtual orbitals. Similar behaviors have been observed for ppRPA@B3LYP calculations and for other defect systems, as shown in the SI. Thus, we choose to use the active space composed of 200 occupied and 200 virtual orbitals in all ppRPA calculations in this work. Compared with the previous work of using the active-space ppRPA approach for molecular systems,[54] the number of orbitals needed in the active space for periodic systems is larger due to denser manifold of low-lying states in solids. Nevertheless, the size of the active space is still much smaller than the full system size.

Table 1: Vertical excitation energies of NV^- in diamond obtained from the ppRPA approach based on PBE and B3LYP functionals compared with reference values. Extrapolated values were obtained from the results of supercells containing 63 and 215 atoms. In ppRPA calculations, the geometry of the $^3A_2$ ground state and cc-pVDZ basis set were used. All values are in eV.

	^1E	$^1A_1$	^3E
Experiment[29,78]	$0.50 \sim 0.59$	$1.76 \sim 1.85$	2.18
ppRPA@PBE (supercell 215)	0.52	1.64	1.92
ppRPA@PBE (extrapolated)	0.53	1.67	1.95
ppRPA@B3LYP (supercell 215)	0.60	1.92	2.09
ppRPA@B3LYP (extrapolated)	0.61	1.97	2.10
TDDFT@PBE[15]	0.51	1.34	2.09
TDDFT@B3LYP	0.69	2.12	2.39
TDDFT@DDH[15]	0.68	1.97	2.37
G_0W_0-BSE@PBE[13]	0.40	0.99	2.32
DMET-NEVPT2[29]	0.53	1.62	2.40
QDET[15]	0.48	1.32	2.16
CRPA+CI[32]	0.49	1.41	2.02

The vertical excitation energies (VEEs) of NV^- in diamond obtained from the ppRPA approach based on PBE and B3LYP using the 215-atom supercell and a two-point extrapolation scheme are presented in Table 1. The extrapolation was done using 63-atom and

215-atom excitation energies in a linear fitting of the form: $E(1/N_{\text{atom}}) = E_\infty + a/N_{\text{atom}}$. As shown in Ref. 15 and Ref. 31, the linear extrapolation with respect to the number of atoms in supercell models has been successfully used to predict vertical excitation energies of defect systems in the thermodynamic limit. We note that, there are uncertainties in the estimation of experimental VEEs. For example, when based on experimental zero-phonon lines (ZPLs) and the Franck-Condon shifts obtained from TDDFT calculations,[15] the VEEs are reported to be $0.40 \sim 0.55$ eV for the ^{1}E state and $1.53 \sim 1.62$ eV for the ^{1}A$_1$ state. It is well-known that TDDFT has an undesired dependence on the exchange-correlation functional. In Table 1, TDDFT@PBE severely underestimates the excitation energy of the ^{1}A$_1$ state, while TDDFT@B3LYP and TDDFT@DDH overestimate excitation energies of all excited states by $0.1 \sim 0.4$ eV. G_0W_0-BSE@PBE underestimates the excitation energy of the ^{1}A$_1$ state by 0.8 eV and has errors around 0.1 eV for other two states. The embedding approaches, including DMET, QDET, and CRPA+CI, predict accurate excitation energies for low-lying ^{1}E and ^{3}E states. However, QDET and CRPA+CI significantly underestimate the excitation energy of the ^{1}A$_1$ state by 0.4 eV or more. In contrast, we find that the ppRPA approach provides a balanced description of all excited states. For three excited states, ppRPA@B3LYP predicts accurate excitation energies with errors around 0.1 eV. The ppRPA approach based on PBE slightly underestimates excitation energies, especially for ^{1}A$_1$ and ^{3}E states, with errors around 0.2 eV. In addition, ppRPA has a weaker DFT starting-point dependence than TDDFT. For instance, the difference between excitation energies of the ^{1}A$_1$ state obtained from ppRPA with the GGA and the hybrid functionals is only 0.3 eV, which is less than half of the 0.8 eV difference between TDDFT@PBE and TDDFT@B3LYP. As shown in Table 1 and in the SI, we also observe that excitation energies for NV^- in diamond have a weak dependence on the size of the supercell model. The difference between ppRPA excitation energies from using the 215-atom supercell and those from the two-point extrapolation is smaller than 0.05 eV.

We now turn to the discussion of SiV^0 in diamond. The vertical excitation energies of

Table 2: Vertical excitation energies of SiV^0 in diamond obtained from the ppRPA approach based on PBE and B3LYP functionals compared with reference values. Experimental vertical excitation energy is estimated by combining the experimental ZPL value of 1.31 eV[78] and the Franck-Condon shift of 0.29 eV from the TDDFT calculation.[15] Extrapolated values were obtained from the results of supercells containing 63 and 215 atoms. In ppRPA calculations, the geometry of the $^3A_{2g}$ ground state and cc-pVDZ basis set were used. All values are in eV.

	$^3A_{2u}$	^3E_u	$^3A_{1u}$
Experiment		1.60	
ppRPA@PBE (supercell 215)	1.47	1.54	1.81
ppRPA@PBE (extrapolated)	1.27	1.30	1.54
ppRPA@B3LYP (supercell 215)	1.54	1.62	1.89
ppRPA@B3LYP (extrapolated)	1.34	1.38	1.62
TDDFT@PBE[15]	1.24	1.28	1.37
TDDFT@B3LYP	1.41	1.50	1.81
TDDFT@DDH[15]	1.49	1.57	1.76
DMET-CASSCF[30]	2.26	2.44	3.16
DMET-NEVPT2[30]	2.39	2.47	2.61
QDET[27]		1.59	1.62

SiV^0 in diamond obtained from the ppRPA approach based on PBE and B3LYP using the 215-atom supercell and those from the two-point extrapolation are presented in Table 2. As shown in Ref. 15, excitation energies of SiV^0 in diamond obtained from the two-point extrapolation show small differences to those obtained from the more sophisticated four-point extrapolation. Here, TDDFT@B3LYP and TDDFT@DDH achieve high accuracy for predicting the excitation energy of the ^3E_u state. On the other hand, TDDFT@PBE underestimates the ^3E_u energy by 0.3 eV. Similar to the prediction of NV^- in diamond, TDDFT shows a starting-point dependence for SiV^0 in diamond, where the difference in excitation energies from different functionals can be as large as 0.4 eV. Among quantum embedding approaches, the QDET approach produces the smallest error of only 0.02 eV. The large errors in DMET-CASSCF and DMET-NEVPT2 may be attributed to the finite-size error and the unsatisfactory treatment of the hybridization between defect orbitals and the environment.[30]

With the supercell model containing 215 atoms, both ppRPA@PBE and ppRPA@B3LYP predict accurate excitation energies for the ^3E_u state with errors smaller than 0.05 eV. However, the extrapolated results give slightly larger errors around $0.2 \sim 0.3$ eV. Compared with TDDFT, the starting-point dependence in ppRPA is largely reduced. The differences of excitation energies obtained from ppRPA based on PBE and B3LYP are smaller than 0.1 eV. Similar to NV^- in diamond, ppRPA using the hybrid functional B3LYP provides better accuracy than ppRPA based on the GGA functional PBE for SiV^0 in diamond.

Table 3: Vertical excitation energies of kk-VV^0 in 4H-SiC obtained from the ppRPA approach based on PBE and B3LYP using the 286-atom supercell. Experimental vertical excitation energy is estimated by combining the experimental ZPL value of 1.10 eV[16] and the Franck-Condon shift of 0.11 eV from the TDDFT calculation.[15] In ppRPA calculations, the geometry of the $^3A_2$ ground state and cc-pVDZ basis set were used. All values are in eV.

	^1E	$^1A_1$	^3E
Experiment			1.21
ppRPA@PBE (supercell 286)	0.28	0.88	1.12
ppRPA@B3LYP (supercell 286)	0.33	1.13	1.23
TDDFT@PBE[15]	0.33	0.90	1.41
TDDFT@B3LYP	0.43	1.58	1.45
TDDFT@DDH[15]	0.42	1.41	1.46
CRPA+CI[32]	0.29	0.88	1.13

We also applied the ppRPA approach to calculate excitation energies of kk-VV^0 in 4H-SiC. The vertical excitation energies of the kk-configuration of VV^0 in 4H-SiC obtained from the ppRPA approach based on PBE and B3LYP are shown in Table 3. TDDFT with all functionals overestimates the excitation energy of the ^3E state by around 0.2 eV. Compared with TDDFT, CRPA+CI provides improved accuracy with an underestimation of 0.1 eV for the excitation energy of the ^3E state. As shown in Ref. 79, it is more challenging to extrapolate the excitation energies of kk-VV^0 in 4H-SiC with respect to the supercell size. Thus, we only include excitation energies obtained from ppRPA using the supercell model containing 286 atoms in Table 3. ppRPA@PBE shows similar results to CRPA+CI with an

error of 0.1 eV. ppRPA@B3LYP gives the best prediction for the ^{3}E state with an error of only 0.02 eV. We note that, however, with finite size extrapolation, the ppRPA-predicted ^{3}E excitation energy will likely decrease slightly.

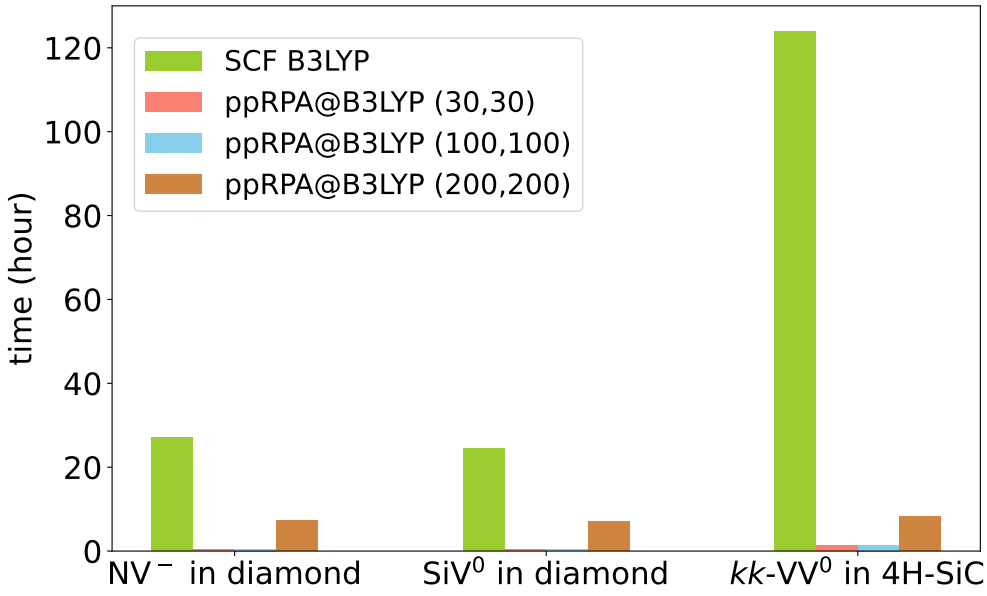

Figure 2: Wall time comparison for the ground-state B3LYP SCF calculations and ppRPA@B3LYP calculations with different active spaces. All calculations were performed on a 48-core CPU node. The supercell model containing 215, 215, and 286 atoms was used for NV^- in diamond, SiV^0 in diamond, and kk-VV^0 in 4H-SiC, respectively. (O, V) means that O occupied orbitals and V virtual orbitals were used in the active space.

In addition to good accuracy for predicting excitation energies of point defects, ppRPA combined with the active-space formalism has a favorable computational scaling. The wall time comparison for the ground-state B3LYP SCF calculations and ppRPA@B3LYP calculations with different active spaces are demonstrated in Fig. 2. The computational cost for ppRPA with 60 or 200 orbitals (including AO to MO transformation and ppRPA steps) is negligible compared to the ground-state SCF for the $(N + 2)$-electron system. At such low cost, reasonably accurate excitation energy prediction can already be obtained from the ppRPA calculations (e.g., with 100 occupied and 100 virtual orbitals). Even for a larger active space with 200 occupied and 200 virtual orbitals, the computational cost of ppRPA is still much smaller than the ground-state DFT calculation. It is also seen that the com-

putational cost of converged active-space ppRPA calculation is nearly independent of the supercell size. For the tested defect systems, the $(N+2)$-electron systems become closed-shell by adding two electrons to half-occupied defect orbitals, which only need to be described by a spin-restricted calculation. This means that the DFT calculation here is cheaper than spin-unrestricted DFT/HF typically used in TDDFT and quantum embedding approaches, although we do not claim such acceleration is universal in all point defect systems. We would like to point out that ppRPA calculations of $(N+2)$- or $(N-2)$-excited states can be reviewed as an seamless Fock space embedding approach of capturing explicitly the correlated interactions of two particles or two holes in the medium of the N-electron system described with a density functional approximation.[53] It is also interesting to point out that while screening is critical for electron interaction in bulk systems, ppRPA, without the pairing interaction kernel, ignores screening.[42] Yet ppRPA is shown here to describe the excitation of point defect well. This is likely due to the cancellation of error, as the ground and excited states of the two particle states have similar localization and screening.

In summary, we applied the ppRPA approach to predict accurate excitation energies of point defects in semiconductors and insulators. In ppRPA calculations, the ground-state SCF calculation for $(N+2)$-electron system is first performed, then excitation energies can be efficiently obtained with an active space consisting only 200 occupied and 200 virtual orbitals. The size of the active space that provides converged excitation energies is shown to be independent of defect systems. For excitations with delocalized characters, we anticipate the required size of the active space may be different. We demonstrated that ppRPA provides a balanced description for different excited states in all tested defect systems including NV^- in diamond, SiV^0 in diamond and kk-VV^0 in 4H-SiC. The errors from ppRPA@B3LYP for predicting excitation energies of the tested point defects are consistently smaller than 0.2 eV. Furthermore, the computational cost of ppRPA is negligible compared with the ground-state DFT calculation when using the active-space formalism. Therefore, we conclude that ppRPA shows promise as an accurate and low-cost tool for investigating excited-state properties of

point defect systems. This work also opens up new opportunities for the application of the ppRPA approach to periodic systems.

Acknowledgement

T.Z. and J.L. are supported by the National Science Foundation (Grant No. CHE-2337991) and a start-up fund from Yale University. J.L. also acknowledges support from the Tony Massini Postdoctoral Fellowship in Data Science. Y.J. acknowledges support from the Midwest Integrated Center for Computational Materials (MICCoM) as part of the Computational Materials Science Program funded by the U.S. Department of Energy, Office of Science, Office of Basic Energy Sciences, under Contract No. DE-AC02-06CH11357. J.Y. and W.Y. acknowledge the support from the National Science Foundation (Grant No. CHE-2154831).

Supporting Information Available

Details about geometry optimization, numerical results of excitation energies obtained from ppRPA in defect systems, basis set convergence for excitation energies obtained from ppRPA.

References

(1) Dreyer, C. E.; Alkauskas, A.; Lyons, J. L.; Janotti, A.; Van de Walle, C. G. First-Principles Calculations of Point Defects for Quantum Technologies. *Annu. Rev. Mater. Res.* **2018**, *48*, 1–26.

(2) Wolfowicz, G.; Heremans, F. J.; Anderson, C. P.; Kanai, S.; Seo, H.; Gali, A.; Galli, G.; Awschalom, D. D. Quantum Guidelines for Solid-State Spin Defects. *Nat Rev Mater* **2021**, *6*, 906–925.

(3) Awschalom, D. D.; Hanson, R.; Wrachtrup, J.; Zhou, B. B. Quantum Technologies with Optically Interfaced Solid-State Spins. *Nat. Photonics* **2018**, *12*, 516–527.

(4) Weber, J. R.; Koehl, W. F.; Varley, J. B.; Janotti, A.; Buckley, B. B.; Van de Walle, C. G.; Awschalom, D. D. Quantum Computing with Defects. *Proc. Natl. Acad. Sci.* **2010**, *107*, 8513–8518.

(5) Jelezko, F.; Gaebel, T.; Popa, I.; Domhan, M.; Gruber, A.; Wrachtrup, J. Observation of Coherent Oscillation of a Single Nuclear Spin and Realization of a Two-Qubit Conditional Quantum Gate. *Phys. Rev. Lett.* **2004**, *93*, 130501.

(6) Anderson, C. P.; Glen, E. O.; Zeledon, C.; Bourassa, A.; Jin, Y.; Zhu, Y.; Vorwerk, C.; Crook, A. L.; Abe, H.; Ul-Hassan, J. et al. Five-Second Coherence of a Single Spin with Single-Shot Readout in Silicon Carbide. *Sci. Adv.* **2022**, *8*, eabm5912.

(7) Christle, D. J.; Klimov, P. V.; de las Casas, C. F.; Szász, K.; Ivády, V.; Jokubavicius, V.; Ul Hassan, J.; Syväjärvi, M.; Koehl, W. F.; Ohshima, T. et al. Isolated Spin Qubits in SiC with a High-Fidelity Infrared Spin-to-Photon Interface. *Phys. Rev. X* **2017**, *7*, 021046.

(8) Ivády, V.; Abrikosov, I. A.; Gali, A. First Principles Calculation of Spin-Related Quantities for Point Defect Qubit Research. *npj Comput Mater* **2018**, *4*, 1–13.

(9) Hohenberg, P.; Kohn, W. Inhomogeneous Electron Gas. *Phys. Rev.* **1964**, *136*, B864–B871.

(10) Parr, R. G.; Weitao, Y. *Density-Functional Theory of Atoms and Molecules*; Oxford University Press, 1989.

(11) Kohn, W.; Sham, L. J. Self-Consistent Equations Including Exchange and Correlation Effects. *Phys. Rev.* **1965**, *140*, A1133–A1138.

(12) Gali, A.; Fyta, M.; Kaxiras, E. Ab Initio Supercell Calculations on Nitrogen-Vacancy Center in Diamond: Electronic Structure and Hyperfine Tensors. *Phys. Rev. B* **2008**, *77*, 155206.

(13) Ma, Y.; Rohlfing, M.; Gali, A. Excited States of the Negatively Charged Nitrogen-Vacancy Color Center in Diamond. *Phys. Rev. B* **2010**, *81*, 041204.

(14) Delaney, P.; Greer, J. C.; Larsson, J. A. Spin-Polarization Mechanisms of the Nitrogen-Vacancy Center in Diamond. *Nano Lett.* **2010**, *10*, 610–614.

(15) Jin, Y.; Yu, V. W.-z.; Govoni, M.; Xu, A. C.; Galli, G. Excited State Properties of Point Defects in Semiconductors and Insulators Investigated with Time-Dependent Density Functional Theory. *J. Chem. Theory Comput.* **2023**, *19*, 8689–8705.

(16) Jin, Y.; Govoni, M.; Wolfowicz, G.; Sullivan, S. E.; Heremans, F. J.; Awschalom, D. D.; Galli, G. Photoluminescence Spectra of Point Defects in Semiconductors: Validation of First-Principles Calculations. *Phys. Rev. Mater.* **2021**, *5*, 084603.

(17) Jin, Y.; Govoni, M.; Galli, G. Vibrationally Resolved Optical Excitations of the Nitrogen-Vacancy Center in Diamond. *npj Comput Mater* **2022**, *8*, 1–9.

(18) Gao, W.; da Jornada, F. H.; Del Ben, M.; Deslippe, J.; Louie, S. G.; Chelikowsky, J. R. Quasiparticle Energies and Optical Excitations of 3C-SiC Divacancy from *GW* and *GW* plus Bethe-Salpeter Equation Calculations. *Phys. Rev. Mater.* **2022**, *6*, 036201.

(19) Choi, S.; Jain, M.; Louie, S. G. Mechanism for Optical Initialization of Spin in NV^- Center in Diamond. *Phys. Rev. B* **2012**, *86*, 041202.

(20) Gallo, A.; Hummel, F.; Irmler, A.; Grüneis, A. A Periodic Equation-of-Motion Coupled-Cluster Implementation Applied to F-centers in Alkaline Earth Oxides. *J. Chem. Phys.* **2021**, *154*, 064106.

(21) Simula, K. A.; Makkonen, I. Calculation of the Energies of the Multideterminant States of the Nitrogen Vacancy Center in Diamond with Quantum Monte Carlo. *Phys. Rev. B* **2023**, *108*, 094108.

(22) Sun, Q.; Chan, G. K.-L. Quantum Embedding Theories. *Acc. Chem. Res.* **2016**, *49*, 2705–2712.

(23) Cui, Z.-H.; Zhu, T.; Chan, G. K.-L. Efficient Implementation of Ab Initio Quantum Embedding in Periodic Systems: Density Matrix Embedding Theory. *J. Chem. Theory Comput.* **2020**, *16*, 119–129.

(24) Zhu, T.; Cui, Z.-H.; Chan, G. K.-L. Efficient Formulation of Ab Initio Quantum Embedding in Periodic Systems: Dynamical Mean-Field Theory. *J. Chem. Theory Comput.* **2020**, *16*, 141–153.

(25) Zhu, T.; Chan, G. K.-L. Ab Initio Full Cell GW+DMFT for Correlated Materials. *Phys. Rev. X* **2021**, *11*, 021006.

(26) Ma, H.; Govoni, M.; Galli, G. Quantum Simulations of Materials on Near-Term Quantum Computers. *npj Comput Mater* **2020**, *6*, 1–8.

(27) Ma, H.; Sheng, N.; Govoni, M.; Galli, G. Quantum Embedding Theory for Strongly Correlated States in Materials. *J. Chem. Theory Comput.* **2021**, *17*, 2116–2125.

(28) Sheng, N.; Vorwerk, C.; Govoni, M.; Galli, G. Green's Function Formulation of Quantum Defect Embedding Theory. *J. Chem. Theory Comput.* **2022**, *18*, 3512–3522.

(29) Haldar, S.; Mitra, A.; Hermes, M. R.; Gagliardi, L. Local Excitations of a Charged Nitrogen Vacancy in Diamond with Multireference Density Matrix Embedding Theory. *J. Phys. Chem. Lett.* **2023**, *14*, 4273–4280.

(30) Mitra, A.; Pham, H. Q.; Pandharkar, R.; Hermes, M. R.; Gagliardi, L. Excited States

of Crystalline Point Defects with Multireference Density Matrix Embedding Theory. *J. Phys. Chem. Lett.* **2021**, *12*, 11688–11694.

(31) Verma, S.; Mitra, A.; Jin, Y.; Haldar, S.; Vorwerk, C.; Hermes, M. R.; Galli, G.; Gagliardi, L. Optical Properties of Neutral F Centers in Bulk MgO with Density Matrix Embedding. *J. Phys. Chem. Lett.* **2023**, *14*, 7703–7710.

(32) Bockstedte, M.; Schütz, F.; Garratt, T.; Ivády, V.; Gali, A. Ab Initio Description of Highly Correlated States in Defects for Realizing Quantum Bits. *npj Quant Mater* **2018**, *3*, 1–6.

(33) Muechler, L.; Badrtdinov, D. I.; Hampel, A.; Cano, J.; Rösner, M.; Dreyer, C. E. Quantum Embedding Methods for Correlated Excited States of Point Defects: Case Studies and Challenges. *Phys. Rev. B* **2022**, *105*, 235104.

(34) Lau, B. T. G.; Busemeyer, B.; Berkelbach, T. C. Optical Properties of Defects in Solids via Quantum Embedding with Good Active Space Orbitals. 2023.

(35) Romanova, M.; Weng, G.; Apelian, A.; Vlček, V. Dynamical Downfolding for Localized Quantum States. *npj Comput Mater* **2023**, *9*, 1–9.

(36) Ring, P.; Schuck, P. *The Nuclear Many-Body Problem*; Springer-Verlag: New York, 1980.

(37) Ripka, S. R. P. G.; Blaizot, J.-P.; Ripka, G. *Quantum Theory of Finite Systems*; MIT Press, 1986.

(38) van Aggelen, H.; Yang, Y.; Yang, W. Exchange-Correlation Energy from Pairing Matrix Fluctuation and the Particle-Particle Random-Phase Approximation. *Phys. Rev. A* **2013**, *88*, 030501.

(39) van Aggelen, H.; Yang, Y.; Yang, W. Exchange-Correlation Energy from Pairing Matrix

Fluctuation and the Particle-Particle Random Phase Approximation. *J. Chem. Phys.* **2014**, *140*, 18A511.

(40) Yang, Y.; van Aggelen, H.; Yang, W. Double, Rydberg and Charge Transfer Excitations from Pairing Matrix Fluctuation and Particle-Particle Random Phase Approximation. *J. Chem. Phys.* **2013**, *139*, 224105.

(41) ROWE, D. J. Equations-of-Motion Method and the Extended Shell Model. *Rev. Mod. Phys.* **1968**, *40*, 153–166.

(42) Peng, D.; van Aggelen, H.; Yang, Y.; Yang, W. Linear-Response Time-Dependent Density-Functional Theory with Pairing Fields. *J. Chem. Phys.* **2014**, *140*, 18A522.

(43) Bohm, D.; Pines, D. A Collective Description of Electron Interactions. I. Magnetic Interactions. *Phys. Rev.* **1951**, *82*, 625–634.

(44) Ren, X.; Rinke, P.; Joas, C.; Scheffler, M. Random-Phase Approximation and Its Applications in Computational Chemistry and Materials Science. *J Mater Sci* **2012**, *47*, 7447–7471.

(45) Peng, D.; Steinmann, S. N.; van Aggelen, H.; Yang, W. Equivalence of Particle-Particle Random Phase Approximation Correlation Energy and Ladder-Coupled-Cluster Doubles. *J. Chem. Phys.* **2013**, *139*, 104112.

(46) Scuseria, G. E.; Henderson, T. M.; Bulik, I. W. Particle-Particle and Quasiparticle Random Phase Approximations: Connections to Coupled Cluster Theory. *J. Chem. Phys.* **2013**, *139*, 104113.

(47) Bannwarth, C.; Yu, J. K.; Hohenstein, E. G.; Martínez, T. J. Hole–Hole Tamm–Dancoff-approximated Density Functional Theory: A Highly Efficient Electronic Structure Method Incorporating Dynamic and Static Correlation. *J. Chem. Phys.* **2020**, *153*, 024110.

(48) Yu, J. K.; Bannwarth, C.; Hohenstein, E. G.; Martínez, T. J. Ab Initio Nonadiabatic Molecular Dynamics with Hole–Hole Tamm–Dancoff Approximated Density Functional Theory. *J. Chem. Theory Comput.* **2020**, *16*, 5499–5511.

(49) Yang, Y.; van Aggelen, H.; Steinmann, S. N.; Peng, D.; Yang, W. Benchmark Tests and Spin Adaptation for the Particle-Particle Random Phase Approximation. *J. Chem. Phys.* **2013**, *139*, 174110.

(50) Yang, Y.; Peng, D.; Lu, J.; Yang, W. Excitation Energies from Particle-Particle Random Phase Approximation: Davidson Algorithm and Benchmark Studies. *J. Chem. Phys.* **2014**, *141*, 124104.

(51) Yang, Y.; Dominguez, A.; Zhang, D.; Lutsker, V.; Niehaus, T. A.; Frauenheim, T.; Yang, W. Charge Transfer Excitations from Particle-Particle Random Phase Approximation—Opportunities and Challenges Arising from Two-Electron Deficient Systems. *J. Chem. Phys.* **2017**, *146*, 124104.

(52) Al-Saadon, R.; Sutton, C.; Yang, W. Accurate Treatment of Charge-Transfer Excitations and Thermally Activated Delayed Fluorescence Using the Particle–Particle Random Phase Approximation. *J. Chem. Theory Comput.* **2018**, *14*, 3196–3204.

(53) Zhang, D.; Yang, W. Accurate and Efficient Calculation of Excitation Energies with the Active-Space Particle-Particle Random Phase Approximation. *J. Chem. Phys.* **2016**, *145*, 144105.

(54) Li, J.; Yu, J.; Chen, Z.; Yang, W. Linear Scaling Calculations of Excitation Energies with Active-Space Particle–Particle Random-Phase Approximation. *J. Phys. Chem. A* **2023**, *127*, 7811–7822.

(55) Zhang, D.; Peng, D.; Zhang, P.; Yang, W. Analytic Gradients, Geometry Optimization and Excited State Potential Energy Surfaces from the Particle-Particle Random Phase Approximation. *Phys. Chem. Chem. Phys.* **2014**, *17*, 1025–1038.

(56) Yang, Y.; Shen, L.; Zhang, D.; Yang, W. Conical Intersections from Particle–Particle Random Phase and Tamm–Dancoff Approximations. *J. Phys. Chem. Lett.* **2016**, *7*, 2407–2411.

(57) Pinter, B.; Al-Saadon, R.; Chen, Z.; Yang, W. Spin-State Energetics of Iron(II) Porphyrin from the Particle-Particle Random Phase Approximation. *Eur. Phys. J. B* **2018**, *91*, 270.

(58) Chen, Z.; Zhang, D.; Jin, Y.; Yang, Y.; Su, N. Q.; Yang, W. Multireference Density Functional Theory with Generalized Auxiliary Systems for Ground and Excited States. *J. Phys. Chem. Lett.* **2017**, *8*, 4479–4485.

(59) Li, J.; Chen, Z.; Yang, W. Multireference Density Functional Theory for Describing Ground and Excited States with Renormalized Singles. *J. Phys. Chem. Lett.* **2022**, *13*, 894–903.

(60) Zhang, D.; Su, N. Q.; Yang, W. Accurate Quasiparticle Spectra from the T-Matrix Self-Energy and the Particle–Particle Random Phase Approximation. *J. Phys. Chem. Lett.* **2017**, *8*, 3223–3227.

(61) Li, J.; Chen, Z.; Yang, W. Renormalized Singles Green's Function in the T-Matrix Approximation for Accurate Quasiparticle Energy Calculation. *J. Phys. Chem. Lett.* **2021**, *12*, 6203–6210.

(62) Orlando, R.; Romaniello, P.; Loos, P.-F. The Three Channels of Many-Body Perturbation Theory: GW, Particle–Particle, and Electron–Hole T-matrix Self-Energies. *J. Chem. Phys.* **2023**, *159*, 184113.

(63) Loos, P.-F.; Romaniello, P. Static and Dynamic Bethe–Salpeter Equations in the T-matrix Approximation. *J. Chem. Phys.* **2022**, *156*, 164101.

(64) Tahir, M. N.; Ren, X. Comparing Particle-Particle and Particle-Hole Channels of the Random Phase Approximation. *Phys. Rev. B* **2019**, *99*, 195149.

(65) Casida, M. E. *Recent Advances in Density Functional Methods*; Recent Advances in Computational Chemistry; WORLD SCIENTIFIC, 1995; Vol. Volume 1; pp 155–192.

(66) Ullrich, C. A. *Time-Dependent Density-Functional Theory: Concepts and Applications*; OUP Oxford, 2011.

(67) Stratmann, R. E.; Scuseria, G. E.; Frisch, M. J. An Efficient Implementation of Time-Dependent Density-Functional Theory for the Calculation of Excitation Energies of Large Molecules. *J. Chem. Phys.* **1998**, *109*, 8218–8224.

(68) Perdew, J. P.; Burke, K.; Ernzerhof, M. Generalized Gradient Approximation Made Simple. *Phys. Rev. Lett.* **1996**, *77*, 3865–3868.

(69) Carnimeo, I.; Affinito, F.; Baroni, S.; Baseggio, O.; Bellentani, L.; Bertossa, R.; Delugas, P. D.; Ruffino, F. F.; Orlandini, S.; Spiga, F. et al. Quantum ESPRESSO: One Further Step toward the Exascale. *J. Chem. Theory Comput.* **2023**, *19*, 6992–7006.

(70) Giannozzi, P.; Baseggio, O.; Bonfà, P.; Brunato, D.; Car, R.; Carnimeo, I.; Cavazzoni, C.; de Gironcoli, S.; Delugas, P.; Ferrari Ruffino, F. et al. Quantum ESPRESSO toward the Exascale. *J. Chem. Phys.* **2020**, *152*, 154105.

(71) Sun, Q.; Berkelbach, T. C.; Blunt, N. S.; Booth, G. H.; Guo, S.; Li, Z.; Liu, J.; McClain, J. D.; Sayfutyarova, E. R.; Sharma, S. et al. PySCF: The Python-based Simulations of Chemistry Framework. *WIREs Comput. Mol. Sci.* **2018**, *8*, e1340.

(72) Sun, Q.; Zhang, X.; Banerjee, S.; Bao, P.; Barbry, M.; Blunt, N. S.; Bogdanov, N. A.; Booth, G. H.; Chen, J.; Cui, Z.-H. et al. Recent Developments in the PySCF Program Package. *J. Chem. Phys.* **2020**, *153*, 024109.

(73) Becke, A. D. Density-functional Thermochemistry. III. The Role of Exact Exchange. *J. Chem. Phys.* **1993**, *98*, 5648–5652.

(74) Lee, C.; Yang, W.; Parr, R. G. Development of the Colle-Salvetti Correlation-Energy Formula into a Functional of the Electron Density. *Phys. Rev. B* **1988**, *37*, 785–789.

(75) Dunning, T. H. Gaussian Basis Sets for Use in Correlated Molecular Calculations. I. The Atoms Boron through Neon and Hydrogen. *J. Chem. Phys.* **1989**, *90*, 1007–1023.

(76) Weigend, F.; Köhn, A.; Hättig, C. Efficient Use of the Correlation Consistent Basis Sets in Resolution of the Identity MP2 Calculations. *J. Chem. Phys.* **2002**, *116*, 3175–3183.

(77) Li, J.; Yu, J.; Yang, W. unpublished.

(78) Davies, G.; Hamer, M. F.; Price, W. C. Optical Studies of the 1.945 eV Vibronic Band in Diamond. *Proc. R. Soc. Lond. Math. Phys. Sci.* **1997**, *348*, 285–298.

(79) Davidsson, J.; Ivády, V.; Armiento, R.; Son, N. T.; Gali, A.; Abrikosov, I. A. First Principles Predictions of Magneto-Optical Data for Semiconductor Point Defect Identification: The Case of Divacancy Defects in 4H–SiC. *New J. Phys.* **2018**, *20*, 023035.